DEVELOPMENT OF YTTRIUM DOPED LEAD TUNGSTATE CRYSTAL FOR PHYSICS APPLICATIONS

Q. DENG, J.Y. LIAO, D.Z. SHEN, D.S. YAN, Z.W. YIN
Shanghai Institute of Ceramics, 1295 Dingxi Road, Shanghai 200050, P.R. China

R.H. MAO, X.D. QU[†], L.Y. ZHANG AND R.Y. ZHU
California Institute of Technology, Pasadena, CA 91125, USA

In this paper we present results of the development of yttrium doped lead tungstate crystal at Shanghai Institute of Ceramics. The crystal growth by modified Bridgman method is described. The segregation coefficient of yttrium ions in lead tungstate crystals was determined. The scintillation emission and transmittance spectra, light output, decay kinetics, light response uniformity and radiation induced color centers were measured. It is found that yttrium doping suppresses the slow scintillation component and improve crystal's radiation resistance.

1. Introduction

Because of its high density, small radiation length and Molière radius and fast decay time, lead tungstate ($PbWO_4$) crystal has attracted wide attention in high energy and nuclear physics community. The Compact Muon Solenoid (CMS) experiment will use 11.2 m^3 large size (25 X_0) $PbWO_4$ crystals for its precision electromagnetic calorimeter (ECAL) at the Large Hadronic Collider (LHC)[1]. The Alice experiments at CERN, the BTeV experiment at Fermilab and the CLAS and PrimEx experiments[2] at CEBAF will also use $PbWO_4$ crystals.

Among all features, a good radiation resistance is required in many of the above applications. An effort has been made at Shanghai Institute of Ceramics (SIC) in the last six years to develop radiation hard lead tungstate crystal with fast decay time for physics applications. Our previous studies have shown that the radiation damage in $PbWO_4$ is caused by the host structure defects, such as oxygen vacancies[3], which introduce local charge imbalance, trap electrons or holes and consequently form color centers under irradiation. One approach to reduce the density of the host structure defects is the optimization of the

[†] Now at Imperial College, University of London, London, United Kingdom.

stoichiometric ratio between two oxides and control it during the crystal growing process. This approach was attempted by SIC as well as other groups[4,5]. It is found this optimization alone was not sufficient. Various approaches to suppress or compensate the remaining defects were taken. Oxygen compensation, referring to post growth annealing at high temperature in an oxygen rich atmosphere, was found to be effective[6], indicating the main mechanism of the radiation damage in $PbWO_4$ is oxygen vacancies, i.e. caused by electron centers.

Doping during crystal growth is another common approach to either artificially introduce local charge imbalance and thus compensate structure defects or function as scavenger to further eliminate unwanted impurities. In development of BGO for the L3 experiment, Eu doping was used at SIC to improve its radiation hardness[7]. In development of CsI(Tl) for the *BaBar* and BELLE experiments, a special scavenge was used at SIC to remove oxygen contamination[6]. Pentavalent (niobium) doping in $PbWO_4$ was first reported by Lecoq *et al.* to be effective in improving transmittance at 100 ppm level[8]. Trivalent (La) doping was first reported by Kobayashi *et al.* to be effective in improving both transmittance[9] and radiation hardness[10]. Consequent studies on doping with various ions, such as La, Lu, Gd, Y and Nb, at optimized level were reported to be effective in improving in transmittance as well as radiation resistance[11,12].

Along the same direction, doping was extensively studied at SIC[13,14,15]. This paper presents growth of yttrium doped $PbWO_4$ crystals by modified Bridgman method at SIC and discusses their optical properties and radiation hardness measured at Caltech as well as SIC.

2. Crystal Growth

$PbWO_4$ single crystals were grown by Modified Bridgman technique at SIC. Raw materials of high purity, PbO (5N) and WO_3 (4N), are produced in Shanghai, and are mixed in precise stoichiometric proportion in an agate mortar. The mixture is first melted in a platinum crucible in air for a period of time to ensure complete homogeneity. After heated to high temperature this melt is sintered into platinum crucible to form polycrystalline $PbWO_4$ grogs for crystal growth.

Figure 1 is a schematic showing typical structure of a modified Bridgman crucible used for the growth of $PbWO_4$ crystals at SIC. The detailed layout of the furnace and its temperature profile can be found in reference[16]. Furnaces of this kind were early developed at SIC to grow BGO for the L3 experiment, and were later successfully adapted to grow CsI(Tl) crystals for two B factories experiments *BaBar* and BELLE.

Crystal were grown along the c axis at SIC. Twenty eight crucibles of rectangular shape are constructed in every furnaces for $PbWO_4$ crystal growth. The shape of crucible makes efficient use of raw materials since only a small fraction of ingot is needed to be cut off to make final dimension. As-grown $PbWO_4$ crystals are transparent, colorless without visible defects, such as cracking, inclusions, scattering centers and growth striation.

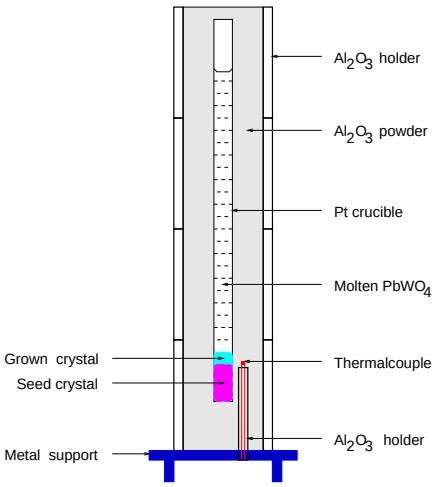

Figure 1. A schematic of the modified Bridgman-Stockbarger crucible used for $PbWO_4$ growth at SIC.

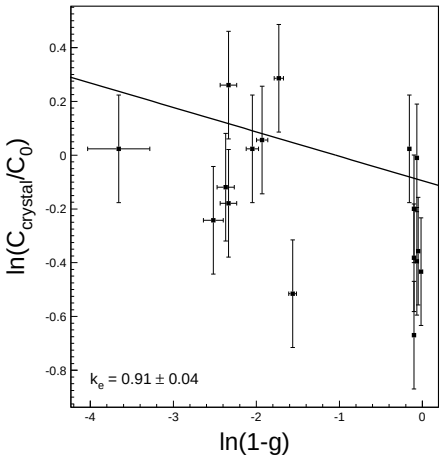

Figure 2. A linear fit of yttrium concentration in $PbWO_4$ crystals.

Table 1. Yttrium concentration (ppmw) in $PbWO_4$ samples

ID	699	699	723	723	727	727	743	743
Melt (ppmw)	29.3	29.3	29.3	29.3	29.3	29.3	29.3	29.3
Z (cm)	5.5	29.0	3.0	26.5	4.0	28.0	4.5	28.0
yttrium (ppmw)	39	29	38	30	30	24	31	20

Table 1 lists the yttrium concentration (ppmw), obtained by Glow Discharge Mass Spectroscopy (GDMS) analysis in four pairs of yttrium doped samples taken at positions Z (cm) from the top (the tail end) of the ingot. Also listed is the initial yttrium concentration (ppmw) in the melt (Melt). The data in Table 1 was used to extract the segregation coefficient of yttrium in $PbWO_4$. According to the equation 4 in reference[14], the logarithmic plot of $C_{crystal}/C_0$ versus $1-g$ is a straight line and its slope and intercept at

$g = 0$ provide a measure of the segregation coefficient k_e, where C_0 is the initial dopant concentration in the melt, $C_{crystal}$ is the dopant concentration in the crystal and g is the relative solidification coefficient, defined as the ratio of the volume of solidification part of the ingot to the whole volume of the melt. Figure 2 shows a linear fit to the GDMS data. The numerical result of the effective segregation coefficient of the yttrium ions in $PbWO_4$ crystal is found to be 0.91 ± 0.04. This rather uniform distribution of the yttrium concentration in $PbWO_4$ crystals makes it a good dopant.

3. Crystal Properties

Optical properties of yttrium doped $PbWO_4$ crystals were characterized at Caltech and SIC. All samples are full size of more than 20 radiation length, typically 2.6 cm $\times$ 2.6 cm at the large end, tapering to 2.2 cm $\times$ 2.2 cm at the small end, and 23 cm long.

3.1. *Emission*

Yttrium doped $PbWO_4$ samples have a broad emission spectrum with a peak at about 420 nm, and the radio luminescence is 15 to 25 nm red shifted as compared to that of the photo luminescence as shown in Figure 3. This red shift is explained by the internal absorption since $PbWO_4$ transmittance at shorter wavelengths is poorer than that at longer wavelengths. A cross check of

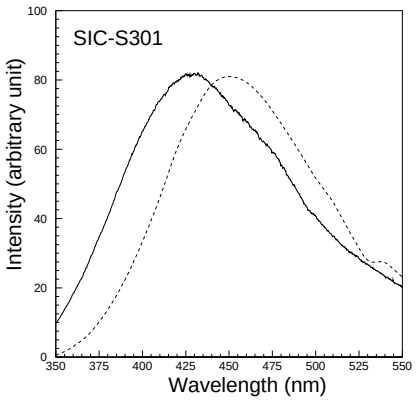

Figure 3. A comparison of photo (solid lines) and radio (dashed lines) luminescence spectra for sample S301.

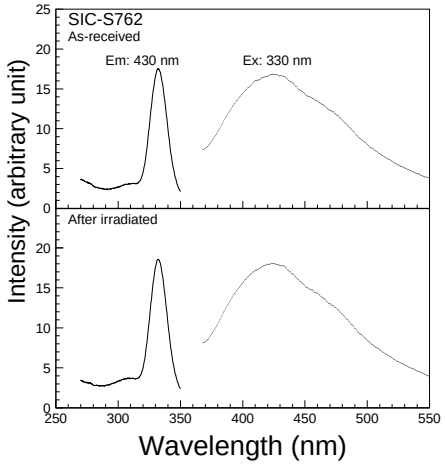

Figure 4. Excitation and photo luminescence spectra are shown before and after γ-ray irradiations at 9 krad/h for sample S762.

photo luminescence with luminescence light passed through the sample showed similar red shift, and thus confirmed this explanation. Since the photo luminescence spectrum shown in Figure 3 is not affected by the internal absorption, it can be seen as the intrinsic emission spectrum, while the radio luminescence spectrum is a convolution of the intrinsic emission and the internal absorption with later depends on the light path[15]. It is interesting to note that both the excitation and emission spectra of $PbWO_4$ crystals is not affected by γ-ray irradiation. Figures 4 shows the excitation and photo luminescence spectra before and after irradiations at 9 krad/h for samples S762. Within the measurement errors the shape of these spectra are identical. This observation consists with our previous conclusion that the scintillation mechanism in $PbWO_4$ crystals is not damaged by the γ-ray irradiation[17,3].

3.2. *Transmittance and Birefringence*

$PbWO_4$ crystal has a birefrigent scheelite crystallographic structure. While its a and b axes are equivalent, its c axis is the symmetry axis. The transmittance measured with light propagating along the c axis (ordinary component only) is different from that measured with light propagating perpendicular to the c axis, which may have a mix of ordinary and extraordinary polarization components. Figure 5 shows transverse and longitudinal transmittance for a sample U517. Also shown in these figures are the theoretical limits of the transmittance calculated by using the refractive index of the ordinary light, propagating

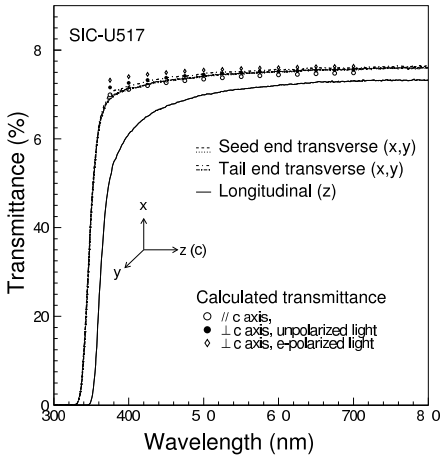

Figure 5. Transverse and longitudinal transmittance of sample U517.

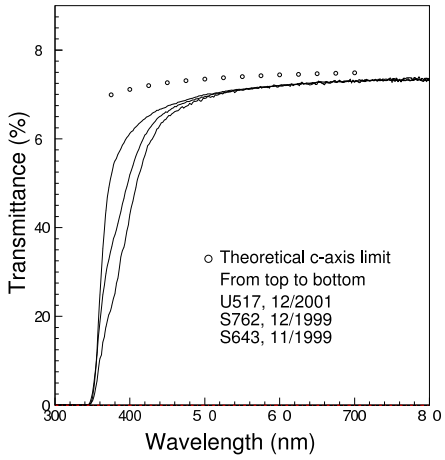

Figure 6. Progress of longitudinal transmittance of three $PbWO_4$ samples.

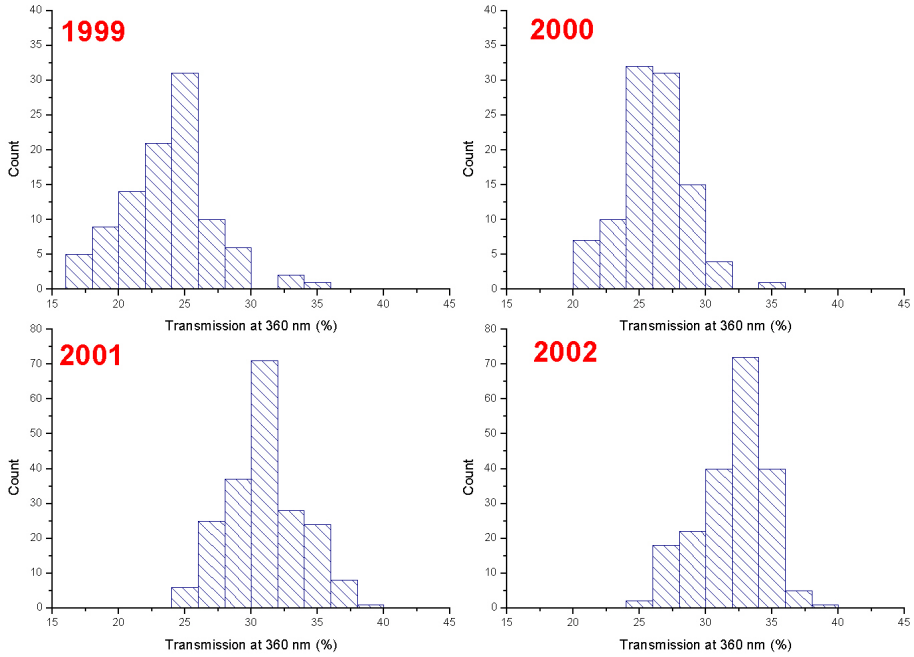

Figure 7. Progress of longitudinal transmittance at 360 nm.

along the c axis, extraordinary polarized light and unpolarized light, propagating perpendicular to the c axis, assuming no internal absorption[17,18]. At the emission peak, 420 nm, the transmittance of the extraordinary polarized light is about 3% higher than that of the ordinary light. The $PbWO_4$ specification on the transmittance, aiming at setting a limit on the internal absorption, thus is crystal orientation dependent, i.e. the transmittance specification along the c axis should be lower than that along the direction perpendicular to the c axis to allow the same density of absorption centers. Since $PbWO_4$ crystals are grown along the c axis at SIC, the difference between the longitudinal and transverse transmittance shown in Figures 5 reflects the internal absorption integrated over the light path as well as the birefringence. It is also interesting to note that the transverse transmittance curves measured in two directions perpendicular to the c axis at both the seed and tail ends are almost identical, indicating that (1) $PbWO_4$ crystals grown along the c axis is isotropic transversely and (2) this sample has very good longitudinal uniformity.

Figure 6 shows the longitudinal transmittance as a function of wavelength for three $PbWO_4$ samples produced at different time. Also shown in the figure is the theoretical limit of transmittance along the c axis. As seen from the

figure that recent grown crystals approach theoretical limit, indicating very low residual absorption. Early samples have a low transmittance at short wavelength caused by scattering centers, but no direct correlations between transmittance and the radiation hardness were observed. A fine tuning of growth parameters improved transmittance at short wavelength, as shown in Figure 6 and 7, where statistical distribution of longitudinal transmittance at 360 nm is presented for crystals grown in 1999 to 2002.

3.3. *Light Output and Decay Kinetics*

Full size (25 radiation lengths) yttrium doped $PbWO_4$ crystals produces typically 10 p.e. per MeV energy deposition. It has also a -2%/°C temperature dependence. Stringent control of temperature and its correction are thus necessary to achieve 1% precision in light output measurement[15]. Figures 8 shows light output as a function of integrated time for three yttrium doped $PbWO_4$ samples. Data in these plots are in units of number of photo electrons per MeV of energy deposition (p.e./MeV). The ratio between light outputs integrated to 100 and 1,000 ns is about 95%, as compared to 90% and 85% for Sb doped and undoped $PbWO_4$ crystals respectively[14].

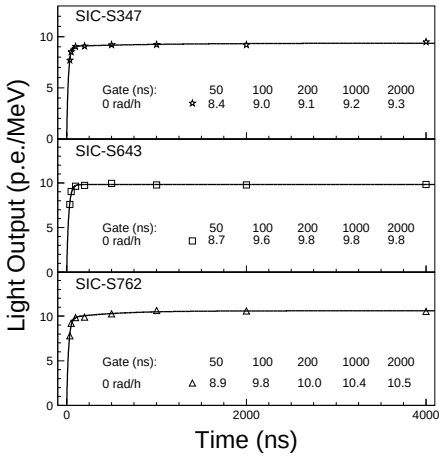

Figure 8. Light output is shown as a function of integration time for three samples.

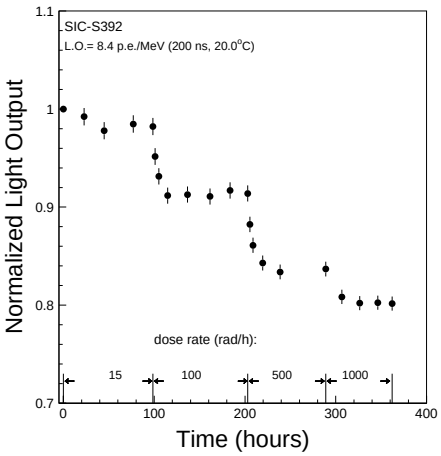

Figure 9. Normalized light output is shown as a function of time under irradiations for a sample S392.

3.4. *Light Output Degradation under Irradiation*

The light output, however, degrades under irradiation. It is known that radiation induced color centers are created in $PbWO_4$ crystals by irradiation, and may annihilate in room temperature. During irradiation, both annihilation and creation processes coexist, the color center density reaches an equilibrium at a level depending on the dose rate applied[6]. Figures 9 shows light output normalized to that before irradiation (solid dots with error bars) as a function of time under irradiation for samples S392. The light output was defined as an average of nine measurements with a collimated ^{137}Cs source shooting at evenly distributed positions along the sample to properly evaluate the degradation of light output and reduce systematic uncertainty. Measurements were done step by step for different dose rates: 15, 100, 500 and 1,000 rad/h, as shown in these figures. The degradation of the light output shows a clear dose rate dependence, as described in reference[6].

Table 2. Summary of light output measurements

Sample	L.O. (1/MeV)		Fraction(%)		L.O.(%)@R(rad/h)			
ID	p.e.	γ	$\frac{50ns}{1\mu s}$	$\frac{100ns}{1\mu s}$	15	100	500	1000
S301	9.4	63.5	92.0	96.6	96.6	87.3	79.5	74.3
S347	9.9	66.9	91.3	97.8	95.1	88.6	82.1	78.0
S392	8.4	56.8	92.0	97.3	98.2	91.3	83.6	80.2
S412	8.3	56.1	94.6	98.6	98.2	91.2	85.9	85.3
S643	8.9	60.1	88.8	98.9	88.3	79.8	–	–
S762	10.6	71.6	85.6	94.2	91.5	84.2	81.4	–
606	10.4	70.3	88.3	98.4	91.7	79.3	–	–
678	10.4	70.3	85.2	93.5	94.2	76.0	59.6	–
679	10.8	73.0	85.0	94.7	93.5	73.5	57.3	–
L411	11.7	79.1	71.8	94.0	88.3	79.2	72.3	–
U517	10.3	69.6	70.8	93.2	87.0	71.6	62.7	–
LS614	8.6	58.2	87.2	97.6	98.1	89.5	84.6	–
LS615	9.9	66.9	82.8	96.9	89.7	80.9	76.1	–
U685	11.4	81.4	91.3	97.9	90.4	–	–	–
U686	10.8	77.1	92.1	97.5	98.5	–	–	–
U688	11.1	79.3	90.5	95.5	91.9	–	–	–
U689	10.4	74.3	92.6	96.3	95.5	–	–	–
U690	12.3	87.9	90.1	96.5	92.7	–	–	–
U691	10.8	77.1	91.8	97.7	94.7	–	–	–
U692	10.5	75.0	92.0	98.5	93.2	–	–	–

Table 2 summarizes the numerical results of the light output before irradiation and the normalized light output (%) in equilibrium under certain dose rates. The light output (L.O.), in units of number of photoelectrons per MeV energy deposit (p.e./MeV), is defined as the average of nine measurements

with an integration time of 200 ns at 20.0°C. By using emission weighted quantum efficiencies of the R2059 PMT (14.8%), the measured light output was converted to the light yield in units of photons/MeV.

3.5. *Light Response Uniformity*

While variations of the amplitude of the light output can be inter calibrated, the loss of the energy resolution, caused by the degradation of light response uniformity is not recoverable[3]. To preserve crystal's intrinsic energy resolution the light response uniformity thus must be kept within tolerance. The light response uniformity was measured by moving a collimated γ-ray source along the longitudinal axis of a sample at nine points evenly distributed along the crystal and the response (y) was fit to a linear function,

$$\frac{y}{y_{mid}} = 1 + \delta(x/x_{mid} - 1), \tag{1}$$

where y_{mid} represents the light response at the middle of the crystal, δ represents the deviation of the light response uniformity, and x is the distance from the small (front) end of a tapered crystal.

Figures 10 shows the light response uniformity as a function of accumulated dose for samples S412, where δ is a measure of the light response uniformity, as defined in equation 1. These figures show clearly that the slope (δ) and the shape of the uniformity does not change. This good uniformity can be attributed to the fact that the light attenuation length at the emission peak

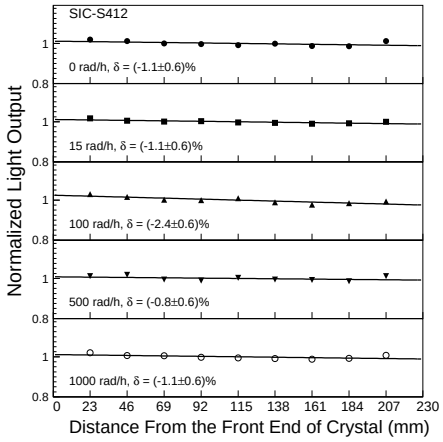

Figure 10. The light response uniformities are shown as a function of integrated dose for sample S412.

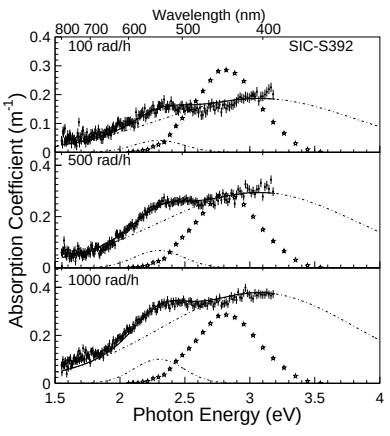

Figure 11. Radiation induced color center density for sample S392.

(420 nm) is long enough even after irradiation, so provides an adequate compensation between the attenuation and the focusing effect caused by crystal's tapered shape[3].

3.6. *Radiation Induced Color Centers*

The longitudinal transmittance data can be used to calculate radiation induced color center density. Figures 11 shows radiation induced color center density as function of photon energy measured for samples S392 in equilibrium at different dose rates. The stars in these figures represent corresponding radio luminescence spectra weighted with quantum efficiency of the PMT. The points with error bars in these figures are radiation induced color center density (D), or absorption coefficient, measured in equilibrium under dose rates specified. They were calculated according to an equation

$$D = 1/LAL_{equilibrium} - 1/LAL_{before}. \tag{2}$$

where LAL is light attenuation length calculated by using longitudinal transmittance according to Equation 1 of reference[17], and the subscript "equilibrium" and "before" refer to "in equilibrium" and "before irradiation" respectively. The radiation induced color center density was decomposed to a sum (solid line) of two color centers with Gaussian shape in photon energy (dashed lines):

$$D = \sum_{i=1}^{2} A_i e^{-\frac{(E-E_i)^2}{2\sigma_i^2}} \tag{3}$$

where E_i, σ_i and A_i denote the energy, width and amplitude of the color center i, and E is photon energy. As seen from these figures, the two center Gaussian fit provides a rather good description of the radiation induced color center data with good χ^2/DoF.

Table 3 lists numerical results of fits for yttrium doped $PbWO_4$ samples. Consistent fit with two common radiation induced color centers at the same energy and with the same width was found for all samples. One broad center is at wavelength of 400 nm (3.07 eV) with a width of 0.76 eV, and other narrow center is at a longer wavelength of 540 nm (2.30 eV) with a width of 0.19 eV. This observation is similar to what observed in doped BGO samples[19], where three common radiation induced absorption bands were observed for BGO samples doped with different dopants, indicating that the radiation induced color centers are presumably not impurity specific rather lattice structure related. This observation also consists with our previous assumption[17,20] that the oxygen vacancies, which are lattice structure defects, are responsible for radiation damage in $PbWO_4$ crystals.

Table 3. Summary of radiation induced color centers

ID	E_1/σ_1 eV/eV	A_1^a m^{-1}	A_1^b m^{-1}	A_1^c m^{-1}	A_1^d m^{-1}	E_2/σ_2 eV/eV	A_2^a m^{-1}	A_2^b m^{-1}	A_2^c m^{-1}	A_2^d m^{-1}
S301	2.30/0.19	0.00	0.04	0.07	0.11	3.07/0.76	0.10	0.22	0.35	0.42
S347	2.30/0.19	0.00	0.00	0.03	0.07	3.07/0.76	0.10	0.13	0.14	0.38
S392	2.30/0.19	0.00	0.04	0.06	0.10	3.07/0.76	0.10	0.18	0.29	0.37
S412	2.30/0.19	0.00	0.03	0.04	0.06	3.07/0.76	0.10	0.15	0.19	0.24
S643	2.30/0.19	0.02	0.05	0.08	–	3.07/0.76	0.14	0.22	0.25	–
S762	2.30/0.19	0.00	0.00	0.00	–	3.07/0.76	0.11	0.21	0.24	–
606	2.30/0.19	0.00	0.07	0.14	–	3.07/0.76	0.10	0.26	0.54	–
678	2.30/0.19	0.03	0.11	0.23	–	3.07/0.76	0.10	0.38	0.78	–
679	2.30/0.19	0.05	0.14	0.26	–	3.07/0.76	0.10	0.39	0.77	–
L411	2.30/0.19	0.01	0.08	0.10	–	3.07/0.76	0.13	0.43	0.54	–
U517	2.30/0.19	0.01	0.09	0.10	–	3.07/0.76	0.17	0.47	0.48	–
LS615	2.30/0.19	0.02	0.07	0.07	–	3.07/0.76	0.13	0.27	0.29	–

^{a,b,c,d} represent 15, 100, 500, 1000 rad/h respectively.

3.7. *Stability*

One peculiar property was found in yttrium doped $PbWO_4$ samples in early development stage. The light output of some yttrium doped samples was found to increase under irradiations. Figure 12 shows the variation of the light output of an early sample after various irradiation and annealing processes. As shown in the figure, its light output was increased by 12% under irradiation at 15 rad/h, and was increased further after a thermal annealing at 100°C. It was

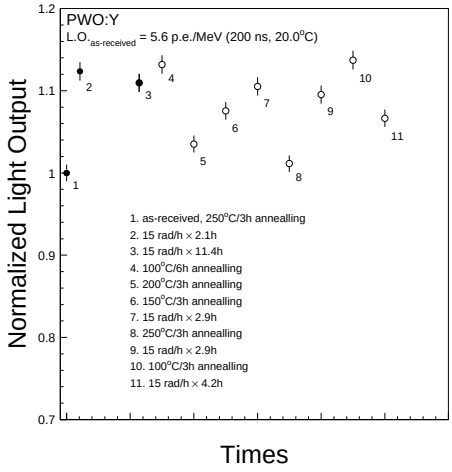

Figure 12. Normalized light output after various irradiation and annealing processes for an early sample.

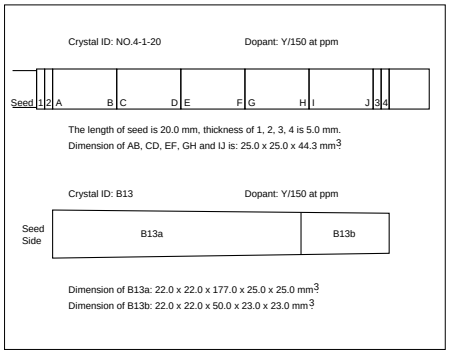

Figure 13. Samples investigated in hunting for the origin of the "instability".

decreased by 10% after a thermal annealing at 200°C. It was also observed that the variations of the light output of these samples correspond to the variations of their transmittance. While showing good light output under irradiations, crystals of this type are not conventional since it is difficult to define their nominal light output.

This peculiarity was understood as the effect of pre-existing color center in early crystals shown in Figure 6, and corresponding self optical bleaching by scintillation light, similar to the BaF_2 crystal case discussed in reference[21]. Scintillation light was produced when a sample is under irradiation by ^{60}Co γ-rays. If the annihilation speed of a pre-existing color center, caused by the bleaching effect of the scintillation light, is larger than the creation speed of a radiation-induced color center under low dose irradiation, the total density of color centers would decrease, not increase, under irradiation[6]. High temperature annealing also creates such pre-existing centers. A study of optical bleaching by using light of different wavelengths confirmed that the optical bleaching is indeed effective in removing pre-existing color centers.

Although an initial thermal annealing at a lower temperature would bypass this problem, R&D was carried out to hunt for the origin of these pre-existing color centers. In this investigation, full size $PbWO_4$ ingots were cut into short

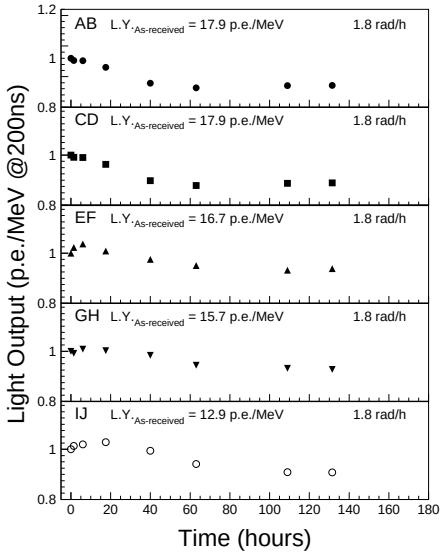

Figure 14. Normalized light output under irradiation at 1.8 rad/h for five 4.4 cm samples cut from ingot 4-1-20.

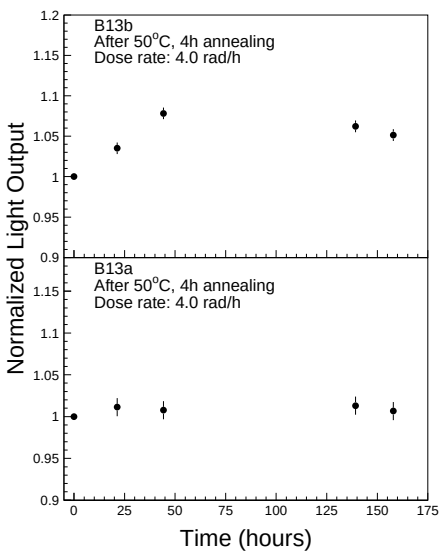

Figure 15. Normalized light output under irradiation at 4 rad/h for 18 and 5 cm samples cut from ingot B13.

pieces. As shown in Figure 13, five $2.5 \times 2.5 \times 4.4$ cm samples were cut from ingot 4-1-20, and an 18 and a 5 cm long samples were cut from another full size tapered sample B13.

All these samples went through standard radiation test at Caltech. It was found that only the sample at the tail end have this problem. Figures 14 and 15 show normalized light output of these short samples under irradiations at low dose rate. No "instability" was found for samples cut from the seed side of ingots. The GDMS analysis results carried out for these samples shows that the impurities of Na, K, Cu, As and Mo were concentrated at the tail end[15].

Following this investigation, several ionic impurities were deliberately added to $PbWO_4$ melt to study the consequence. The result shows that monovalant impurities, such as K^+ and Na^+, enhance pre-existing color center at 420 nm, as shown in Figure 16.

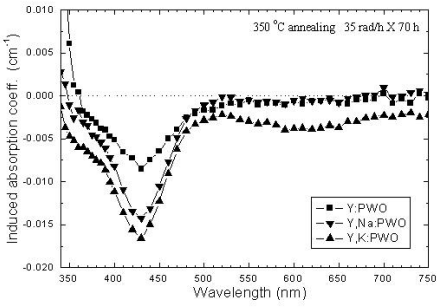

Figure 16. Radiation induced absorption of yttrium, potassium and sodium doped $PbWO_4$ samples.

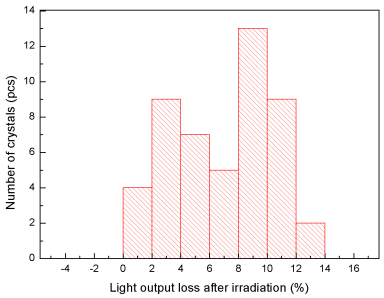

Figure 17. Normalized light output loss after irradiation at 35 rad/h.

As a consequence of this study, limitations to the monovalant impurities were added to the the raw material specification and parameters of crystal growth were modified accordingly. The yttrium doped samples grown at SIC since then are free from this "instability". Figure17 shows a statistical distribution of the light output loss after irradiation at 35 rad/h measured at SIC. No increase of light output was observed. This observation was also confirmed by measurement at Caltech. Correspondingly, the transmittance at 420 nm has also improved, as shown in Figure 18.

4. Summary

Yttrium doping is found to shift the emission to blue, and yttrium doped $PbWO_4$ crystal has a broad spectrum peaked at 420 nm. It is also effective

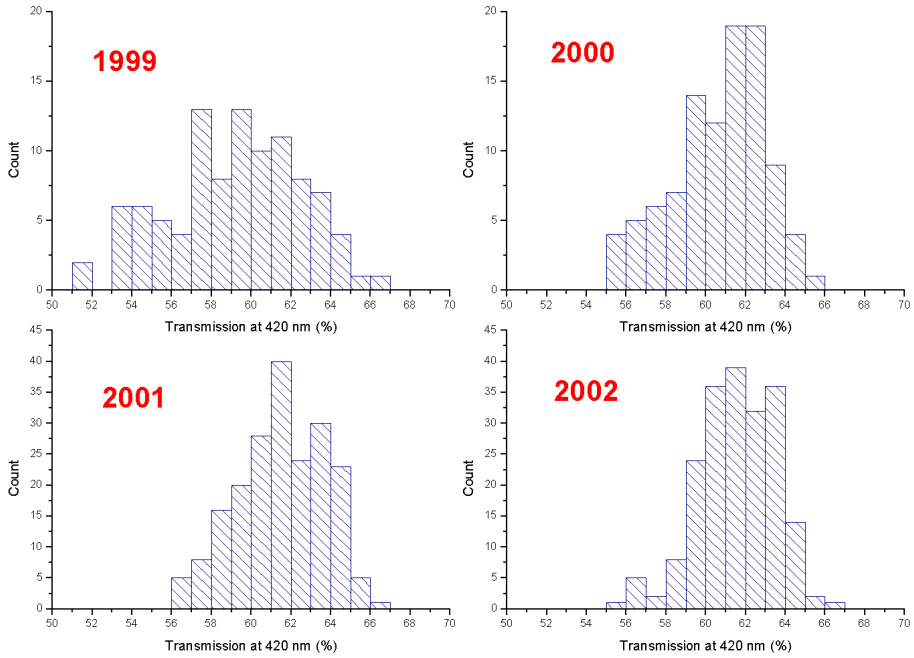

Figure 18. Progress of longitudinal transmittance at 420 nm.

in reducing slow scintillation component, and leading to $PbWO_4$ crystals with adequate radiation hardness for the LHC environment. With yttrium doping it is not necessary to implement oxygen compensation. The concentration of yttrium ions in $PbWO_4$ crystals is rather uniform with a segregation coefficient of 0.91 ± 0.04.

The radiation induced absorption in all samples can be decomposed to two color centers with two common centers peaked at wavelength of 400 nm (3.07 eV) and 540 nm (2.30 eV) with widths of 0.76 and 0.19 eV respectively. These centers are not as deep as that in Sb doped samples[14]. This explains a relatively large dose rate dependence of radiation damage and relatively large damage speed in yttrium doped $PbWO_4$ crystals.

Light output of early yttrium doped $PbWO_4$ samples is sensitive to the temperature of thermal annealing. Pre-existing color centers, which are bleachable by scintillation light, led to the "instability", i.e. the light output increase under irradiations. These pre-existing color centers were found to be caused by impurities at the tail end of ingots, and were formed by contamination of monovalant impurities, such as Na+ and K^+. With refined growth parameters and stringent requirement to the purity of raw material these pre-existing color

centers were eliminated, so that yttrium doped samples grown recently at SIC are free from the "instability".

Acknowledgments

This work is supported in part by U.S. Department of Energy Grant No. DE-FG03-92-ER40701.

References

1. *Compact Muon Solenoid Technical Proposal*, **CERN/LHCC 94-38**, LHCC/P1 (1994).
2. A. Gasparian, in these Proceedings.
3. R.Y. Zhu, *Nucl. Instr. and Meth.* **A413** (1998) 297.
4. A.N.Annenkov *et al.*, **CMS NOTE 1997/055**.
5. M.Nikl *et al.*, *J.Appl.Phys.***82** (1997) 5758.
6. R.Y. Zhu, *IEEE Trans. Nucl. Sci.* **NS-44** (1997) 468.
7. Z.Y. Wei *et al.*, *Nucl. Instr. and Meth.* **A297** (1990) 163.
8. P. Lecoq *et al.*, *Nucl. Instr. and Meth.* **A365** (1995) 291.
9. M. Kobayashi *et al.*, *Nucl. Instr. and Meth.* **A399** (1997) 261.
10. M. Kobayashi *et al.*, *Nucl. Instr. and Meth.* **A404** (1998) 149.
11. S.Baccaro *et al.*, *Phys. Stat. Sol.* **A164** (1997) R9.
12. E. Auffray *et al.*, *Nucl. Instr. and Meth.* **A402** (1998) 75.
13. Q. Deng *et al.*, *Nucl. Instr. and Meth.* **A438** (1999) 415.
14. X.D. Qu *et al.*, **A469** (2001) 193.
15. X.D. Qu *et al.*, **A480** (2002) 470.
16. Z.W. Yin *et al.*, *Proc. SCINT99*, Ed. V. Mikhailin, (1999) 206.
17. R.Y. Zhu *et al.*, *Nucl. Instr. and Meth.* **A376** (1996) 319.
18. G. Bakhshiva and A. Morozov, *Sov. J. Opt. Technol* **44** (1977) 9.
19. R.Y. Zhu *et al.*, *Nucl. Instr. and Meth.* **A302** (1991) 69.
20. R.Y. Zhu *et al.*, *IEEE Trans. Nucl. Sci.* **NS-45** (1998) 686.
21. D.A. Ma *et al.*, *Nucl. Instr. and Meth.* **A356** (1995) 309.